J. Fluid Mech. (1982), *vol.* 123, *pp.* 523–535
Printed in Great Britain

A vortex-street model of the flow in the similarity region of a two-dimensional free turbulent jet

By J. W. OLER† AND V. W. GOLDSCHMIDT

School of Mechanical Engineering, Ray W. Herrick Laboratories, Purdue University, West Lafayette, Indiana 47907

(Received 6 April 1981 and in revised form 30 March 1982)

The mean-velocity profiles and entrainment rates in the similarity region of a two-dimensional jet are generated by a simple superposition of Rankine vortices arranged to represent a vortex street. The spacings between the vortex centres, their two-dimensional offsets from the centreline, as well as the core radii and circulation strengths, are all governed by similarity relationships and based upon experimental data.

Major details of the mean flow field such as the axial and lateral mean-velocity components and the magnitude of the Reynolds stress are properly determined by the model. The sign of the Reynolds stress is, however, not properly predicted.

1. Introduction

Recognition of the importance of the large-scale structures in turbulent shear flows dates back to Towsend (1956) and Grant (1958). Most of the current emphasis on this aspect of turbulent fluid mechanics is a result of the experiments conducted in a plane mixing layer by Brown & Roshko (1971, 1974), Winant & Browand (1974) and Browand & Weidman (1976). These investigations have clearly illustrated the presence of large, essentially two-dimensional roller vortices with axis perpendicular to the plane of mean shear. The coherent structures scale on the dimensions of the mean flow, and it is apparent that the growth rate of the mixing layer is controlled by the rate at which the structures coalesce. Both the mixing-layer growth rate and the eddy-coalescence rate are independent of the Reynolds number of the flow.

The strongest indication of a coherent structure in two-dimensional jet flows is the well-documented 'flapping' phenomena. This characteristic is easily detected by measuring the correlation function between the fluctuating longitudinal velocities at symmetric points on either side of the jet centreline. At zero time delay, the correlation is negative, thereby indicating that instantaneous transverse distributions of the velocity fluctuation are on the average asymmetric. For increasing time delays, the correlation function has the alternately positive and negative values that are characteristic of periodic phenomena. This behaviour in two-dimensional jets has been compared to the flapping of a flag in which the centreline of the mean-velocity profile is periodically displaced about its average position. It was thought that the flapping was essentially a travelling-wave instability rather than an indication of a coherent large-scale structure. 'Flapping' two-dimensional jets have been reported by Bradbury (1965), Goldschmidt & Bradshaw (1973), Gutmark & Wygnanski (1976), Everitt & Robins (1978), and Cervantes (1978, 1980).

An alternative explanation for the periodic correlation function is the presence of

† Present Address: Texas Technical University, Lubbock, Texas.

coherent large-scale eddies arranged in a pattern similar to the classical von Kármán vortex street as shown in figure 1. A plane jet flow containing this structure would exhibit instantaneously asymmetric distributions of longitudinal velocity fluctuation and is inherently periodic.

In the detailed measurements by Cervantes (1978), he noted that the streamwise variation of the 'flapping' frequency is compatible with the similarity scaling relationships for a plane jet. Consequently, the 'flapping' frequency F_f, when non-dimensionalized by local mean-velocity scale and lengthscale, is equal to a constant $S_f = F_f b/u_m \approx 0{\cdot}1$. Here the local scales are chosen to be the mean centreline velocity u_m and the jet half-width b. The same observation and determination of the dimensionless frequency were made by Oler & Goldschmidt (1980) from measurements of structural-passage frequency in the intermittent region of a plane jet. Approximate agreement with this value of S_f may also be inferred from the 'flapping' jet investigations by Bradbury (1965), Goldschmidt & Bradshaw (1973), Gutmark & Wygnanski (1976) and Everitt & Robins (1978). This agreement on the dimensionless flapping frequency implies a Reynolds-number independence that was verified by Cervantes. Both the mean-flow scaling of the structural-passage frequency and its Reynolds-number independence bear a strong resemblance to the large-scale structure in plane mixing layers.

Recent flow-visualization experiments by Moallemi (1980) strongly suggest a vortex street pattern of the large structures in a plane jet. By stretching oil-coated smoke wires parallel to and on either side of the jet centreline in the ambient fluid, the silhouette of apparently two-dimensional large eddies could be discerned as the smoke convected into the turbulent–non-turbulent interface. This image is reinforced by two-point correlations of the longitudinal velocity fluctuation reported by Oler & Goldschmidt (1981). When presented in the form of an isocorrelation contour map, the presence of a vortex-street pattern is clearly indicated.

To conclude, there are a number of factors that may be interpreted to suggest that the large-scale structure of a fully developed plane jet is similar to the classical von Kármán vortex street. A numerical simulation of a hypothetical jet characterized by this structure is described in the following sections.

2. A numerical simulation

The similarity region of a two-dimensional jet is simulated with a vortex street structure such as that illustrated in figure 1. By utilizing a linear superposition of Rankine vortices, the velocity at any point in the flow field is determined by the additive effects of all vortices making up the pattern. Although a reasonable approximation might have been to superpose the vortex-street structure onto an otherwise homogeneous mean flow, that approach is not utilized in the present investigation. It is assumed instead that the vortices are themselves totally responsible for the mean-flow field.

The large-scale structures are of principal interest in the simulation, and consequently the smaller turbulent scales have not been modelled directly. However, the small scales and the associated eddy viscosity may be considered as being responsible for the cores of the Rankine vortices.

As was shown from similarity arguments by Oler & Goldschmidt (1980), the number of large structures per unit length in a plane jet should decrease with respect to downstream distance in proportion to $x^{-\frac{5}{2}}$. It is not clear whether this is accomplished through an eddy-coalescence mechanism, as in the plane mixing layer, or simply an

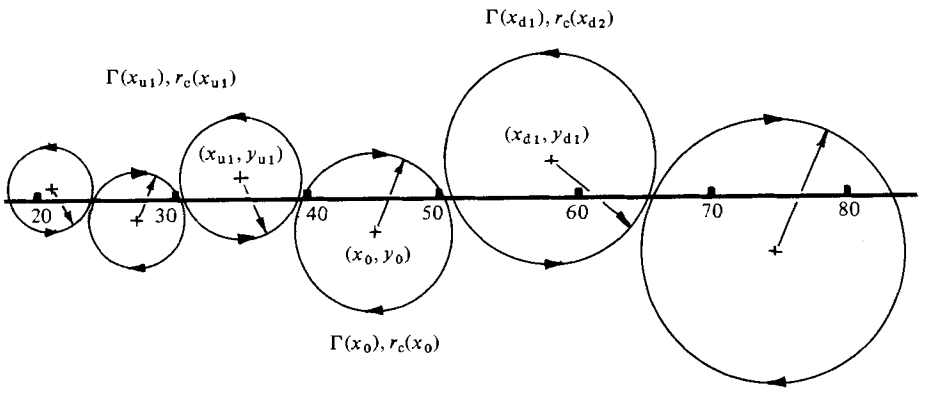

FIGURE 1. A vortex-street representation of a plane jet.

imbalance in the generation and destruction of the large structures. In the numerical simulation, the reduction in the number of vortices with respect to downstream distance is included. However, the contribution of the mechanism of reduction to the calculated flow properties has not been represented in any way. One might suspect that this is a critical omission, since conditionally sampled measurements in the mixing layer have indicated large values of Reynolds-stress production in the region of an eddy-coalescence event.

For the model formulation and calculated results presented herein, all quantities have been made dimensionless by the jet exit conditions, i.e. the slot width D and exit velocity u_0. It is assumed that the jet to be modelled is characterized by spreading and velocity decay rates given by

$$b = \beta x, \tag{2.1}$$

$$u_m = C_m x^{-\frac{1}{2}}, \tag{2.2}$$

where $\beta = 0{\cdot}1$ and $C_m = 2{\cdot}36$.

The basic element of the vortex-street model is a Rankine vortex. These vortices have the classical velocity distribution of a diffusing line vortex given by

$$v_\theta = \frac{\Gamma}{2\pi r}\left\{1-\exp\left[-1{\cdot}26\left(\frac{r}{r_c}\right)^2\right]\right\}. \tag{2.3}$$

Here the core radius has been chosen to coincide with the position of maximum velocity. The net velocity components at a point (x,y) resulting from the linear superposition of N Rankine vortices having coordinates (x_i, y_i) are given by

$$u(x,y) = \sum_{i=1}^{N} -\frac{\eta_i}{r_i} v_{\theta i}, \tag{2.4a}$$

$$v(x,y) = \sum_{i=1}^{N} \frac{\xi_i}{r_i} v_{\theta i}, \tag{2.4b}$$

where $$\xi_i = x-x_i, \quad \eta_i = y-y_i, \quad r_i^2 = \xi_i^2+\eta_i^2.$$

From figure 1, it may be noted that the parameters required to describe the vortex street uniquely are the co-ordinates, radius and strength of each vortex. Since the plane jet is a self-preserving flow and the vortex street is expected to satisfy structural similarity requirements, the descriptive parameters may be defined in terms of global

length and velocity scaling relationships. Specifically, for a plane jet, lengthscales are expected to vary in direct proportion to x, while velocities go as $x^{-\frac{1}{2}}$.

As illustrated in figure 1, one vortex with a negative lateral coordinate is arbitrarily chosen as a reference vortex with coordinates denoted by (x_0, y_0). By applying the similarity-scaling relationships, the lateral coordinate, core radius, and strength of any other vortex may be expressed as

$$y_i = (-1)^{i+1} C_y x_i, \tag{2.5a}$$

$$r_{ci} = C_r x_i, \tag{2.5b}$$

$$\Gamma_i = (-1)^{i+1} C_\Gamma x_i^{\frac{1}{2}}, \tag{2.5c}$$

where x_i is the longitudinal coordinate of the ith upstream x_{ui}, or downstream x_{di} vortex. C_y, C_r, and C_Γ are as-yet undefined proportionality constants.

As the vortices move downstream, the pattern wavelength increases, convective velocities decrease, and the number of vortices per unit length diminishes through coalescence or a similar mechanism. All of these features must be accounted for in the determination of the longitudinal vortex coordinates.

Let u_s and f_s be the vortex convective velocity and passage frequency respectively. The number of vortices per unit length, or vortex density, is

$$n_s = \frac{2f_s}{u_s}, \tag{2.6}$$

where the factor of 2 is a consequence of there being two vortices in each wavelength of the pattern. From similarity considerations,

$$f_s = C_f x^{-\frac{3}{2}}, \tag{2.7a}$$

$$u_s = C_u x^{-\frac{1}{2}}, \tag{2.7b}$$

so that (2.6) may be written as

$$n_s = \frac{2C_f}{C_u} x^{-1}. \tag{2.8}$$

Let the reference vortex be instantaneously located at (x_0, y_0). The number of vortices between x_0 and some downstream station x_d may be found by integrating the vortex density with respect to x. The position of the ith downstream vortex is such that the number of vortices between x_0 and x_{di} is equal to i. Utilizing (2.8) yields

$$i = \int_{x_0}^{x_{di}} \frac{2C_f}{C_u} x^{-1}\, dx, \tag{2.9}$$

or

$$x_{di} = x_0 \exp \frac{iC_u}{2C_f}. \tag{2.10}$$

The position of the ith upstream vortex is found in an analogous manner:

$$x_{ui} = x_0 \exp\left(-\frac{iC_u}{2C_f}\right). \tag{2.11}$$

To summarize, given the instantaneous location of the reference vortex, the longitudinal coordinates of all the other vortices may be found from (2.10) and (2.11). The lateral coordinates, strengths and core radii may then be calculated from (2.5).

The total induced velocity at a point exhibits a time dependence that is governed by the movement of all the vortices making up the vortex street pattern. The time averages of the fluctuating velocity may be found by integrating with respect to time

over one period of the pattern as it passes any transverse plane. When calculating the averages, provision must be made for the streamwise variation of the convective velocity and recombination rate of the vortices.

Consider the convection of vortices past a transverse plane at $\tilde{x}$. During a time interval τ the number of vortices that cross the plane is given by

$$A(\tilde{x}, \tau) = \int_0^\tau u_s n_s \, dt \tag{2.12}$$

or

$$A(\tilde{x}, \tau) = 2C_f \tilde{x}^{-\frac{3}{2}} \tau. \tag{2.13}$$

If $x_0 = \tilde{x}$ at $t = 0$, then the number of vortices that have passed $\tilde{x}$ at $t = \tau$ must be equal to the number of vortices between $\tilde{x}$ and x_0. From (2.9) and (2.13) this equality may be written as

$$\frac{2C_f}{C_u} \ln \frac{x_0}{\tilde{x}} = 2C_f \tilde{x}^{-\frac{3}{2}} \tau, \tag{2.14}$$

or

$$x_0 = \tilde{x} \exp (C_u \tilde{x}^{-\frac{3}{2}} \tau). \tag{2.15}$$

The preceding relationship defines the time-dependent position of the reference vortex given that at $t = 0$ it is located at $x_0 = \tilde{x}$. The position of the other vortices in the structural pattern may be found from (2.10) and (2.11) so that the time dependence of the complete velocity field is determined. Mean values of the flow properties may then be determined by averaging over one wavelength of the vortex-street pattern as it passes $\tilde{x}$ or until the number of vortices between $\tilde{x}$ and x_0 is equal to 2.

As formulated, the numerical simulation requires the specification of five proportionality constants: C_y, C_r, C_Γ, C_f and C_u. These are utilized in similarity relationships to describe the streamwise variation of the vortex lateral coordinate, core radius, strength, passage frequency, and convection velocity.

The passage-frequency and convection-velocity coefficients are set equal to 2·36 and 1·18 respectively, on the basis of experimental data (see Cervantes 1978; Oler & Goldschmidt 1980; Moallemi 1980; Oler 1980). The values for the strength, lateral-coordinate and core-radius coefficients are chosen to be such that the agreement between the calculated and experimentally determined mean-velocity profile at $x = 45$ is optimized. This results in $C_\Gamma = 2{\cdot}597$, $C_y = 0{\cdot}04$ and $C_r = 0{\cdot}13$. It should be noted that Moallemi (1980) has estimated $C_y = 0{\cdot}05$ on the basis of flow-visualization experiments. It should also be emphasized that, once determined, the coefficients are held constant, and the streamwise variations of the vortex street parameters are determined strictly on the basis of the similarity relationships.

3. Simulation results

The mean longitudinal velocity at (x, y) is calculated from

$$\bar{u}(x, y) = \frac{1}{T} \int_0^T u(x, y; t) \, dt. \tag{3.1}$$

The resulting transverse distributions of $\bar{u}(x, y/b)/u_m(x)$ are illustrated in figure 2 for $x = 15$, 30, 45, 60 and 75. Also included in the figure are experimentally determined distributions and the analytical prediction of Reichardt (1943),

$$\frac{\bar{u}}{u_m} = \exp (-0{\cdot}693\eta^2), \tag{3.2}$$

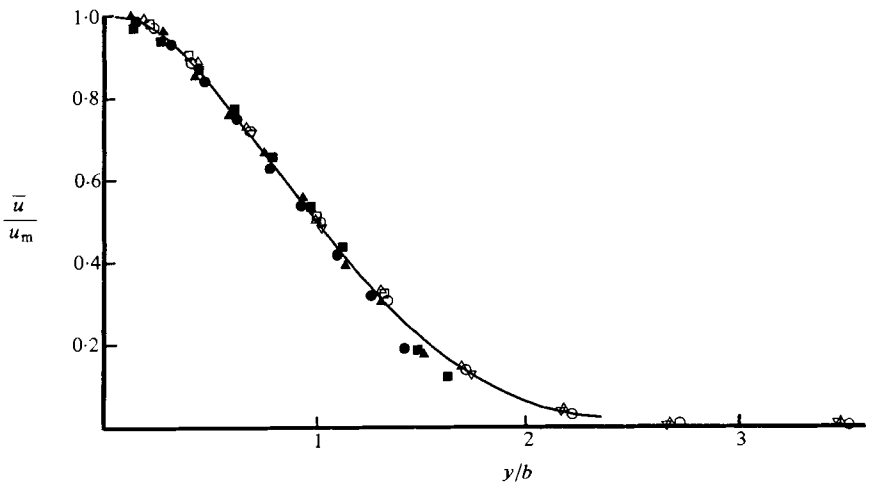

FIGURE 2. Lateral distribution of the mean longitudinal velocity component. Calculated profiles; ○, $x = 15$; □, 30; △, 45; ▽, 60; ◇, 75. Profiles measured with a Pitot tube: ●, $x = 20$; ■, 35; ▲, 50. Theoretical prediction by Reichardt (1943): ——.

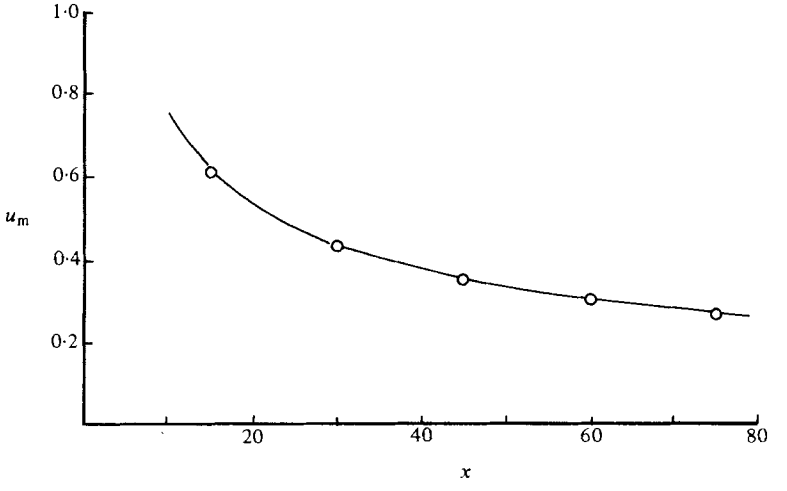

FIGURE 3. Streamwise variation of the mean centreline velocity: ○, calculated; ——, measurements by Oler (1980).

where $\eta = y/\beta x$. The velocity half-width utilized for the scaling of the transverse coordinate is taken to be $b = 0{\cdot}1x$ for both the experimental and calculated distributions.

The collapse of the calculated profiles from the various transverse planes onto the reduced coordinate $\eta = y/b$ supports the manner in which the self-preserving characteristics of real jet flows are incorporated into the jet simulation. To further illustrate the capability of the model to duplicate similarity scaling, the calculated variation of the mean centreline velocity $u_m(x)$ is given in figure 3, along with measured data.

Mean lateral velocities may be calculated numerically from

$$\bar{v}(x, y) = \frac{1}{T}\int_0^T v(x, y; t)\, dt. \tag{3.3}$$

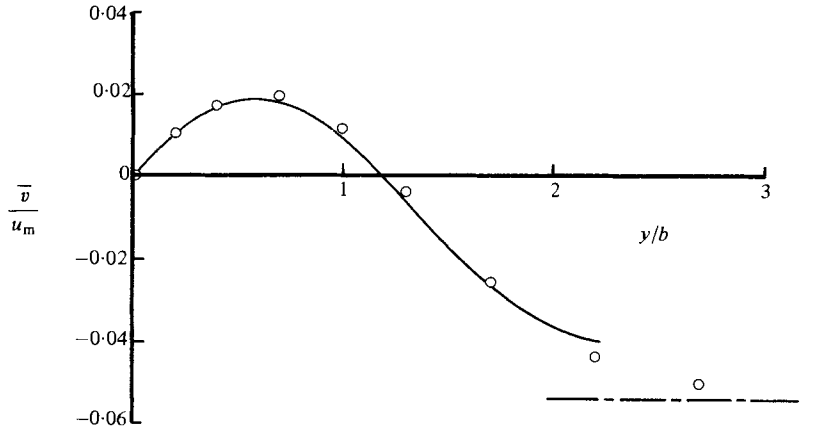

FIGURE 4. Lateral distribution of the mean lateral velocity component: ○, calculated profile; ——, experimentally derived by Gutmark & Wygnanski (1976); — · —, asymptotic limit derived by Townsend (1956).

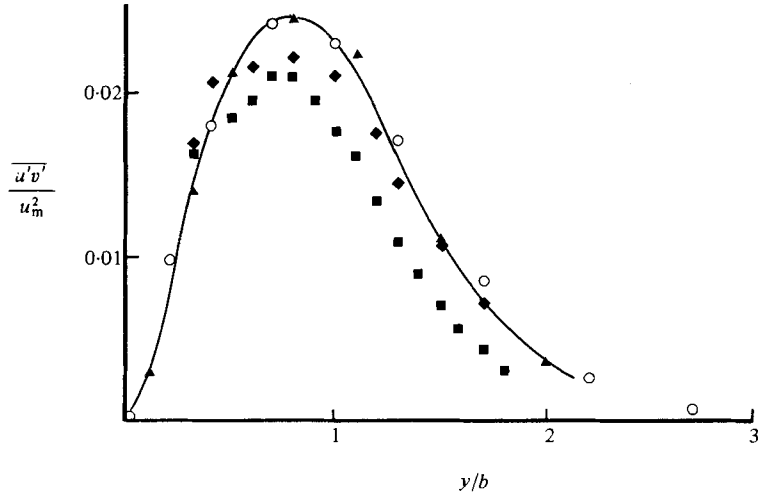

FIGURE 5. Lateral distribution of the Reynolds stress. ○, calculated. Measurements by Jenkins & Goldschmidt (1974): ◆, $x = 35$; ■, 45. Measurements by Gutmark & Wygnanski (1976): ▲, $x = 100$; ——, 100 (derived using (3.6)).

Figure 4 illustrates the resulting transverse distribution $\bar{v}(x, y/b)/u_m(x)$. Also indicated on the figure are the asymptotic value of the entrainment velocity given by Townsend (1956) and the distribution calculated from continuity using $f(\eta)$, the experimentally determined longitudinal velocity distribution, i.e.

$$g(\eta) = \beta\left[-\frac{1}{2}\int_0^\eta f(\eta)\,d\eta + \eta f(\eta)\right], \tag{3.4}$$

where $g(\eta) = \bar{v}/u_m$. The jet-simulation results compare favourably with these.

Local values of the Reynolds stress are calculated as the product of instantaneous velocity fluctuations, i.e.

$$\overline{u'v'}(x, y) = \frac{1}{T}\int_0^T [u(x, y; t) - \bar{u}(x, y)]\,[v(x, y; t) - \bar{v}(x, y)]\,dt. \tag{3.5}$$

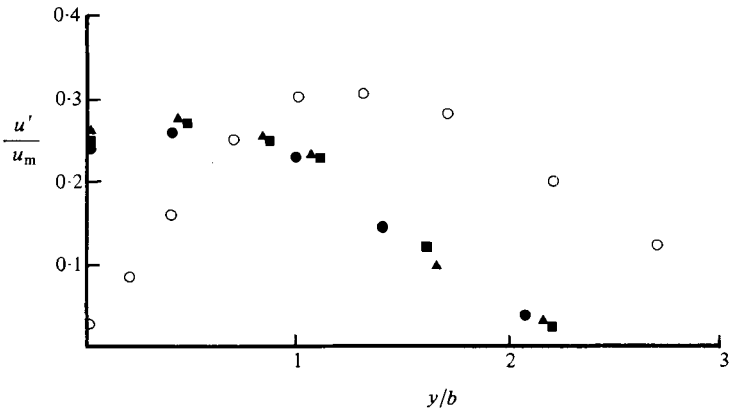

FIGURE 6. Distribution of longitudinal fluctuation intensity. ○, calculated. Measurements by Chambers & Goldschmidt (1982): ●, $x = 20$; ■, 40; ▲, 60.

The resulting distributions of $|\overline{u'v'}(x, y/b)/[u_m(x)]^2|$ are given in figure 5. For comparison, experimentally determined distributions by Jenkins & Goldschmidt (1974) and Gutmark & Wygnanski (1976) are given in the figure. The distribution of Reynolds stress may also be determined by integrating the momentum equation while utilizing the continuity equation, similarity relationships and a mean longitudinal velocity profile. The result is

$$q(\eta) = -\tfrac{1}{2}\beta \int_0^\eta \left[f(\eta)^2 + \frac{df(\eta)}{d\eta}\int_0^\eta f(\eta)\,d\eta\right]d\eta, \tag{3.6}$$

where $q(\eta) = -\overline{u'v'}/u_m^2$. The Reynolds stress determined in this manner is also included in figure 5.

It should be noted that only absolute values are plotted in figure 5. This is a consequence of the inability of the stimulation to predict the correct sign for the Reynolds stress. The simulation predicts negative values of the eddy viscosity $\mu_t = -\rho\overline{u'v'}/(\partial\bar{u}/\partial y)$. The magnitude of the predicted Reynolds stress is, however, easily within the uncertainty limits of the data. It is indeed surprising that the model, which is nothing more than a kinematic simulation of the flow, is capable of predicting the magnitude of a dynamic property of the 'turbulent' field such as the Reynolds stress. The opinion held by the authors is that the incorrect sign for the turbulent shear stress involves a subtle deficiency in the present kinematic representation that can only be overcome through consideration of the dynamics of the energy-transport processes.

'Turbulent' fluctuation intensities are calculated from

$$\frac{\overline{[u'(x,y)^2]}^{\frac{1}{2}}}{u_m(x)} = \frac{1}{u_m(x)}\left\{\frac{1}{T}\int_0^T [u(x,y;t)-\bar{u}(x,y)]^2\,dt\right\}^{\frac{1}{2}} \tag{3.7}$$

and a similar expression for the lateral fluctuations. The calculated distributions are illustrated in figures 6 and 7. As presently formulated, the vortex-street model fails to represent the fluctuating velocity field accurately. Although the calculated distributions are qualitatively reasonable, the magnitudes of the lateral fluctuations are about twice the experimental values, and the longitudinal fluctuations near the axis are much lower than the experimentally determined ones.

These discrepancies are directly related to the neglect of the small-scale turbulence

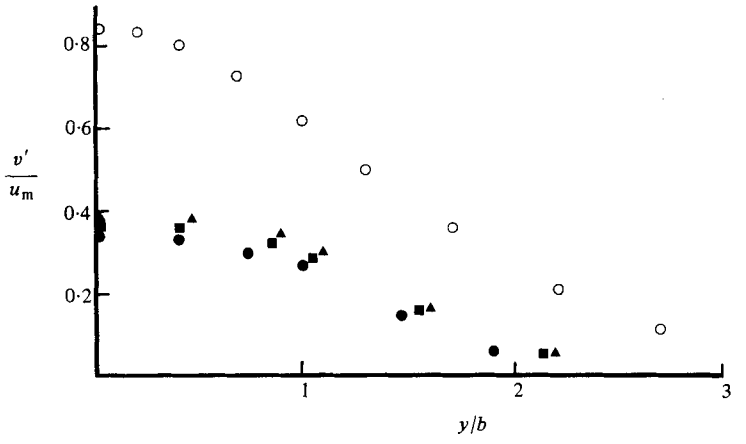

FIGURE 7. Distribution of lateral fluctuation intensity. Symbols as in figure 6.

and the simplicity of the Rankine vortex model. The extremely high values of the lateral fluctuations are a result of the linear superposition of the velocities induced at the midpoint between counter-rotating vortices on opposite sides of the centreline. In these regions, the total velocities are about twice what either vortex would induce alone. Undoubtedly, the inclusion of small-scale turbulent-diffusion effects would limit the unreasonably high local strain rates predicted by the current vortex-street model.

As with the distributions of turbulent-fluctuation intensity, other flow properties that are intimately related to the small-scale fluctuations cannot be predicted by the present model. For instance, the turbulent-kinetic-energy equation cannot be evaluated, since there is no representation of the eddies that accept energy from the large scales or the smallest eddies that provide for the viscous dissipation of energy. Similarly, nothing may be inferred concerning the turbulent-energy spectra, since the model only represents the lowest-frequency components.

4. The mechanisms of entrainment and Reynolds-stress production

On the basis of the calculated results from the vortex-street model, it is apparently the large eddies that are responsible for entrainment and Reynolds-stress production. Insight into the manner in which this is accomplished may be gained by using the model to postulate the flow fields that would exist for jet spreading rates other than the naturally occurring one. An examination of those calculations leads to the conclusion that point values of Reynolds stress and entrainment velocity are a consequence of the streamwise variation in the size, spacing and strength of the large eddies.

Since the spreading rate is incorporated into the vortex-street model as a lengthscale, it is a simple matter to vary the spreading rate and observe the effect on the calculated flow field. For each calculation, the velocity scale is adjusted so that the momentum flux is equal to that of the naturally occurring flow. This leads to

$$bu_m^2 \int_{-\infty}^{+\infty} f(\eta)^2 \, d\eta = \text{constant} \tag{4.1}$$

or

$$\beta C_m^2 = 0{\cdot}1 \times 2{\cdot}36^2. \tag{4.2}$$

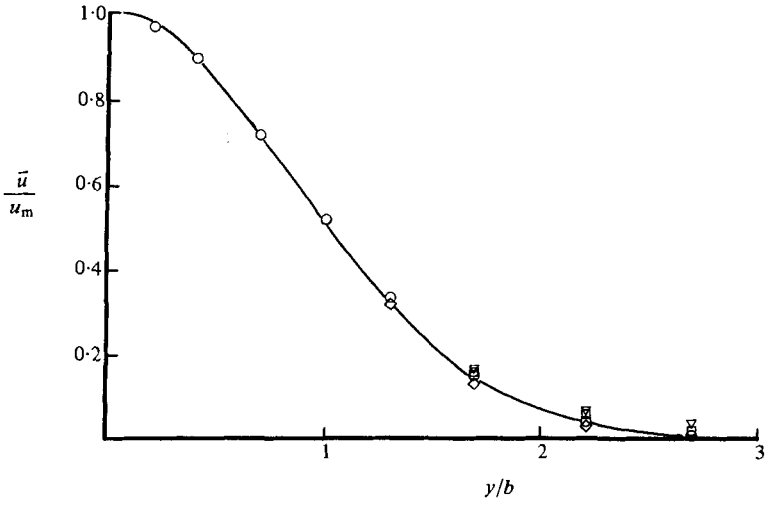

FIGURE 8. Effect of the spreading rate on the mean longitudinal velocity profile. Calculated: ▽, $\beta = 0{\cdot}25$; □, 0·15; ○, 0·10; △, 0·07; ◇, 0·03. Theoretical prediction by Reichardt (1943): ——.

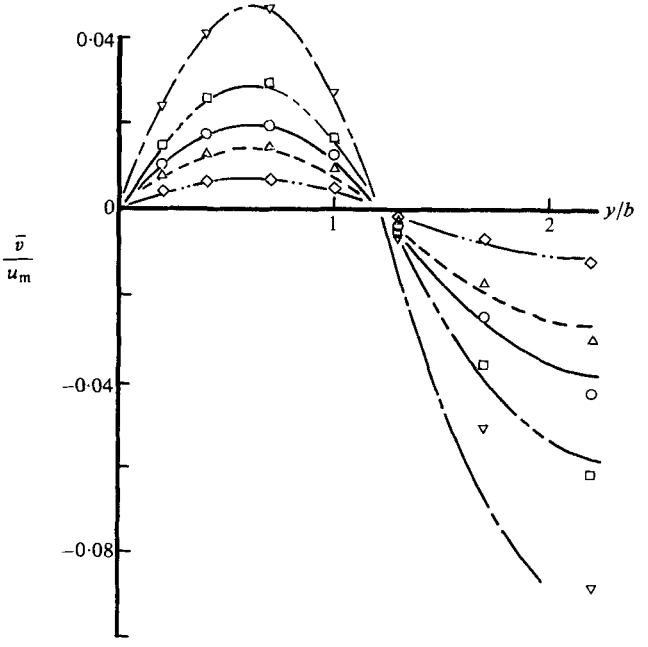

FIGURE 9. Effect of the spreading rate on the mean lateral velocity profile. Results from the stimulation: open symbols as in figure 8. Derived from the self-preserving profile: —·—, $\beta = 0{\cdot}25$; — - - —, 0·15; ——, 0·10; - - - -, 0·07; —··—, 0·03.

For a particular β, C_m is determined from (4.2). Then C_r, C_f, C_Γ, and C_u are changed proportionately from the values that are appropriate for the naturally occurring flow. These proportionality constants are not re-optimized for the postulated spreading rates.

Figures 8, 9 and 10 illustrate calculated distributions of $\bar{u}$, $\bar{v}$ and $\overline{u'v'}$ over a wide

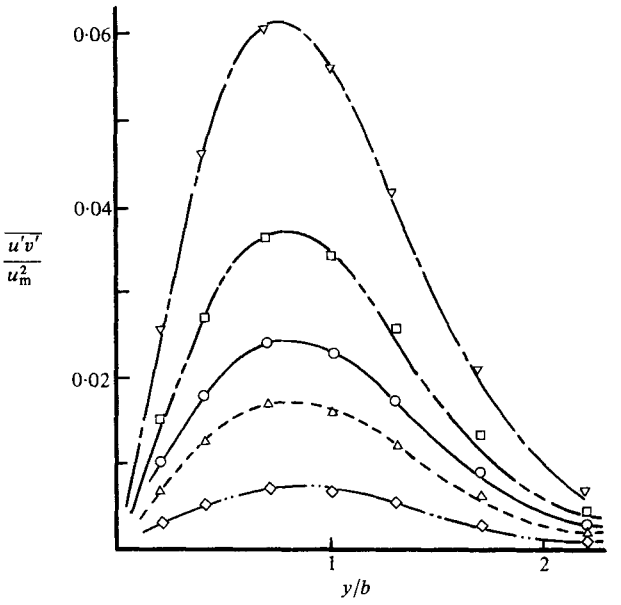

FIGURE 10. Effect of the spreading rate on the Reynolds stress distribution. Symbols as in figure 9.

range of hypothetical spreading rates. For comparison, the corresponding distributions from (3.2), (3.4) and (3.6) are also given. As the spreading rate goes to zero, the mean longitudinal velocity profile is unchanged while the Reynolds stress and lateral velocity uniformly approach zero. This trend to zero illustrates that utilizing a viscous vortex model such as the Rankine vortex and arranging the vortices into a vortex-street pattern do not in themselves force the generation of non-zero averages of turbulent stress and lateral velocity. Furthermore, it is clear that the point averages of these properties are intimately related to the streamwise development of the individual vortices and the vortex street as a whole.

The essential difference between the spreading and non-spreading flows is the relative influence of the large eddies upstream versus those downstream of the particular point of interest. In the hypothetical non-spreading flow, a perfectly symmetric influence is felt, whereas the influence is non-symmetric in a developing flow. The process may be described as follows. First, as a consequence of the inherent instability of the mean-velocity field, a series of large counter-rotating eddies are produced. From their point of origin, the eddies diffuse continuously as they are convected downstream. The individual vortices eventually lose their identity through a decay, break-up or coalescence process, but the generation, diffusion and destruction sequence is continuously repeated. At a fixed point, the simultaneous influences are felt from comparatively small vortices upstream of the point and larger vortices downstream. The net effect of the non-symmetric upstream and downstream influence of each vortex that passes the point is to produce non-zero averages of Reynolds stress and entrainment velocity.

5. Conclusions

A numerical simulation of the vortex-street model for the large-scale structures of a turbulent plane jet has been described. The formulation includes the effects of streamwise flow development through the expression of geometry and vortex parameters in terms of similarity-scaling relationships.

The calculated results indicate that the hypothesized structure is capable of giving virtually exact representations of the velocity decay rate, mean-velocity profiles, and the Reynolds-stress distribution. Although the qualitative shapes of the fluctuation-intensity profiles are reasonable, the magnitudes are in considerable error. This is a consequence of the failure to include the effects of the small-scale turbulence directly.

Unfortunately, the model predicts a negative turbulent viscosity. There is the possibility that the entire concept of a vortex-street structure is invalid. However, this is difficult to accept owing to the experimental evidence, which suggests such a structure, and the capability of the model to predict distributions of $\bar{u}$, $\bar{v}$ and $|\overline{u'v'}|$ accurately. It is suggested that the problem with the Reynolds stress may be resolved through the inclusion of relationships describing the dynamics of the energy-transport processes and that further research be made in this area.

It is evident that the key feature of the vortex-street model is the inclusion of the effects of global flow development on locally measured or calculated turbulent-flow properties. The essential mechanism for the production of Reynolds stress and entrainment appears to be the non-symmetric influence of the upstream and downstream large-scale structures as they diffuse and are convected past a particular point of interest.

The work reported is part of an overall effort funded by the Office of Naval Research (N0014-75-C-1048) and the National Science Foundation (GK 19317h3, Eng. 74-20780). Their support is gratefully acknowledged.

The authors would also like to express their appreciation to the referees for their valuable comments and criticisms.

REFERENCES

Bradbury, L. J. S. 1965 The structure of a self-preserving turbulent plane jet. *J. Fluid Mech.* **23**, 31.

Browand, F. K. & Weidman, P. D. 1976 Large scales in the developing mixing layer. *J. Fluid Mech.* **76**, 127.

Brown, G. L. & Roshko, A. 1971 The effect of density difference on the turbulent mixing layer. *Turbulent Shear Flows, AGARD*-CP-93, 23–1.

Brown, G. L. & Roshko, A. 1974 On density effects and large structure in turbulent mixing layers. *J. Fluid Mech.* **64**, 775.

Cervantes de Gortari, J. G. 1978 An experimental study of the flapping motion of a turbulent plane jet. Ph.D. thesis. School of Mech. Engng, Purdue University.

Cervantes de Gortari, J. G. 1980 The apparent flapping of a turbulent plane jet – further experimental results. *A.S.M.E. Paper* 80-WA-FE-13.

Chambers, F. W. & Goldschmidt, V. W. 1982 Acoustic interaction with a turbulent plane jet – effects on turbulent structure. *A.I.A.A. Paper* 82–0048.

Everitt, K. W. & Robins, A. G. 1978 The development and structure of turbulent plane jets. *J. Fluid Mech.* **88**, 563.

Goldschmidt, V. W. & Bradshaw, P. 1973 Flapping of a plane jet. *Phys. Fluids* **16**, 354.

GRANT, H. L. 1958 The large eddies of turbulent motion. *J. Fluid Mech.* **4**, 149.

GUTMARK, E. & WYGNANSKI, I. 1976 The planar turbulent jet. *J. Fluid Mech.* **73**, 465.

JENKINS, P. E. & GOLDSCHMIDT, V. W. 1974 Study of the intermittent region of a two-dimensional plane jet. *Dept of Mech. Engng, Purdue University, Herrick Lab. Rep.* HL 74-75.

MOALLEMI, K. 1980 Visualization and characterization of a two-dimensional turbulent jet. M.S. thesis, School of Mech. Engng, Purdue University.

OLER, J. W. 1980 Coherent structures in the similarity region of a two-dimensional turbulent jet: a vortex street. Ph.D. thesis, School of Mech. Engng, Purdue University.

OLER, J. W. & GOLDSCHMIDT, V. W. 1980 Interface crossing frequency as a self-preserving flow variable in a turbulent jet. *Phys. Fluids* **23**, 19.

OLER, J. W. & GOLDSCHMIDT, V. W. 1981 Coherent structures in the similarity region of two-dimensional turbulent jets. In *Proc. 3rd Symp. on Turbulent Shear Flows, University of California, Davis.*

REICHARDT, H. 1943 *J. R. Aero. Soc.* **47**, 167.

TOWNSEND, A. A. 1956 *The Structure of Turbulent Shear Flow.* Cambridge University Press.

WINANT, C. D. & BROWAND, F. K. 1974 Vortex pairing: the mechanism of turbulent mixing-layer growth at moderate Reynolds number. *J. Fluid Mech.* **63**, 237.